# Use of nanostructured materials in medical diagnostics

12

*H.-P. Lin, B.-R. Li*
National Chiao Tung University, Hsinchu, Taiwan

## 12.1 Zero-dimensional (0-D) nanostructured materials

### *12.1.1 Introduction*

The term 0-D nanostructured usually refers to spherically shaped nanoparticles with diameters ranging from five to tens of nanometers. Magnetic, gold, and quantum dot (QD) have been widely studied in the medical diagnosis field. Because QDs have some advantageous and unique photophysical properties, scientists are greatly interested in QDs as a potential fluorescent bio-imaging probe for biomedical diagnosis. One advantage is that QDs excited by a single excitation source can exhibit different emission wave lengths that are dependent on the particle size; this is referred to as the quantum confinement effect. The quantum confinement effect is a size-dependent emission caused by an increased confinement of the excitation with a smaller QD size and thus a higher energy bandgap. So we can observe that the QD of the same material exhibits a red fluorescence with a smaller energy bandgap because of the larger QD size, whereas a smaller QD size exhibits a blue fluorescence. Also, the photostability of fluorescence bio-imaging probes is a crucial point of concern. The photostability of QDs is another advantage and is much more stable than other organic dyes.

### *12.1.2 Synthesis*

QDs are colloidal semiconductor nanoparticles with diameters between 1 and 10 nm. The diameter is an important factor in the optical property of QDs. Therefore we focus on how to produce QDs with correct sizes. There are two general methods for synthesizing QDs: top-down processing and bottom-up processing. With top-down processing, a bulk, thinned semiconductor is generally used to produce the QDs, and the facilities include ion implantation, molecular beam epitaxy (MBE), e-beam lithography, and X-ray lithography. In order to achieve the quantum confinement effect, controlling the shape and size of QDs is necessary. On the other hand, with bottom-up processing, colloidal QDs are prepared by chemical reactions that include the wet-chemical and vapor-phase methods [1]. (I) Wet-chemical methods mainly follow conventional precipitation methods containing the parameters of a single solution or a mixture of solutions. With the precipitation process, the nucleation and the limited growth of particles are two main factors controlling the shape and size of QDs. Also, microemulsion, sol-gel [2–4], competitive reaction chemistry, hot-solution decomposition [5–7], sonication, microwave [8], and electrochemistry processes are categorized as wet-chemical

**Nanobiomaterials. https://doi.org/10.1016/B978-0-08-100716-7.00013-1**

**Table 12.1 Summary of types of quantum dots [12]**

| Type | Group | Quantum dots |
|---|---|---|
| Core nanocrystals | III–V | GaAs, InP, InAs, InGaAs, IrGaAs, AlGaAs |
| | II–VI | CdS, CdSe, CdTe, ZnS, ZnSe, ZnTe, HgS, HgSe, HgTe, MgS, MgSe, MgTe |
| | IV–VI | PbS, PbSe, PbTe |
| Core-shell nanocrystals | CdS/ZnSe, CdS/ZnS, CdSe/ZnS, CdSe/CdS, CdTe/ZnS, CdTe/CdS, PbSe/CdSe, CdSeTe/ZnS, CdHgTe/CdS | |

methods. (II) Vapor-phase methods provide the specific layers, which are grown in an atom-by-atom process to produce QDs [9]. Consequently, self-assembly of QDs occurs on the substrate without any patterning [10,11]. For self-assembly of QDs, vapor-phase methods are generally used by MBE, liquid metal ion sources, sputtering, or aggregation of gaseous monomers processes.

Generally, there are two types of QDs: core nanocrystals and core-shell nanocrystals. The core nanocrystals are commonly composed of elements from group III–V, II–VI, or IV–VI of the periodic table [12] (Table 12.1). Core-shell nanocrystals form a layer or a shell of atoms with a higher bandgap outside the core nanocrystals to enhance the photoluminescence (PL) quantum yield and stability of QDs.

### 12.1.3 Property

QDs are semiconductor nanocrystals with unique photophysical properties because of their physical dimensions that are close to or smaller than the exciton Bohr radius [13]. QDs absorb the light with energy higher than bandgap and then induce the recombination of an electron-hole pair, an exciton, to produce the luminescence. QDs display eye-catching photographs of differentially sized QDs under ultraviolet excitation, which produce a bright rainbow of PL, which is the results of high quantum yield ($\Phi = 0.1–0.9$) and large molar extinction coefficients ($10^5–10^7\,M^{-1}\,cm^{-1}$). The spectrum of QDs has a large, effective Stocks shift of more than 100 nm. On the other hand, the quantum confinement effect is a crucial factor and is dependent on the size of the QDs, which affects the PL property. When a bulk material is reduced to nanoscale dimensions, the density between the valence band and the conduction band decreases, thus inducing the emergence of discrete excitonic states [14,15] (Fig. 12.1). For an instance, bulk CdSe exhibit a band gap energy of 1.76 eV and its Bohr excition diameter of 9.6 nm [16], while nanoscale CdSe (c.2–7 nm) have larger band gap energy from 1.9 to 2.8 eV and its PL shifts between 450 and 650 nm [17]. This effect means that the smaller QDs of the same material can exhibit larger energy bandgap and thus emit shorter wavelength (a PL emission in the blue), whereas larger QDs emission in the red. The PL spectra of QDs exhibit a nearly Gaussian shape with a narrow full-width-at-half-maximum (FWHM) of c.20–30 nm and the PL decay is most multiexponential with average lifetime ranging from c.10 to 100 ns. The QDs have narrower FWHM,

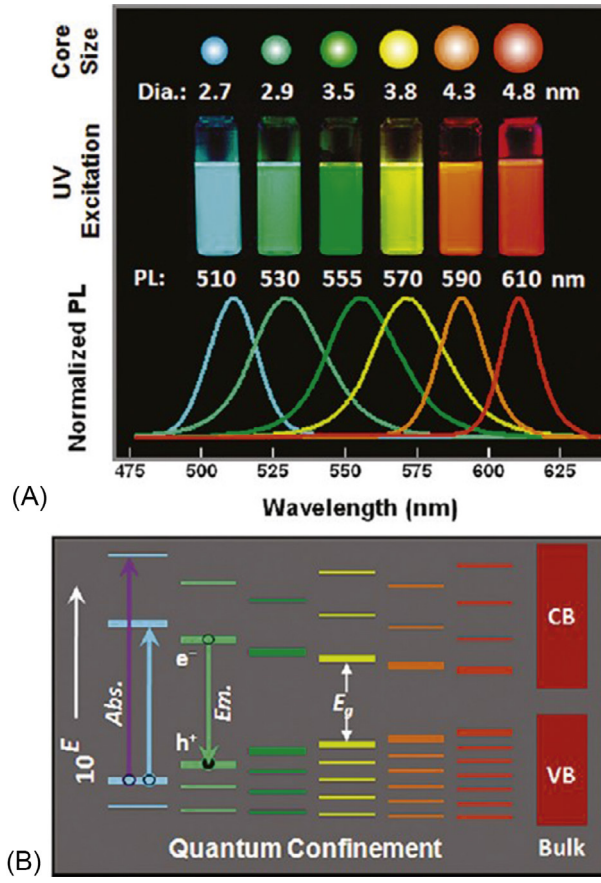


**Fig. 12.1** (A) QDs of the same materials exhibit multiple PL emissions under a single excitation source because the differently sized QDs have different energy bandgaps. The larger energy bandgap of smaller QD emits shorter a wavelength *(closer to blue)*. (B) The quantum confinement of nanoscale QDs has distinct energy levels between the conduction band (CB) and the valence band (VB) of the bulk semiconductor [14].

longer lifetime, and much more stable than the other organic fluorescence dyes for biological applications. Moreover, QDs can display multiple PL emission with a single excitation source (wavelength). This specific photophysical property of QDs has brought numerous interesting in biomedical applications.

### *12.1.4 Surface modification and bioconjugation of QDs*

Because of their unique properties, QDs are usually chosen as the materials for versatile biomedical applications. However, QDs are a type of inorganic material that does not easily solute with water. Thus for biomedical applications, core and core-shell QDs require chemical modification on their outside surface in order to improve their water

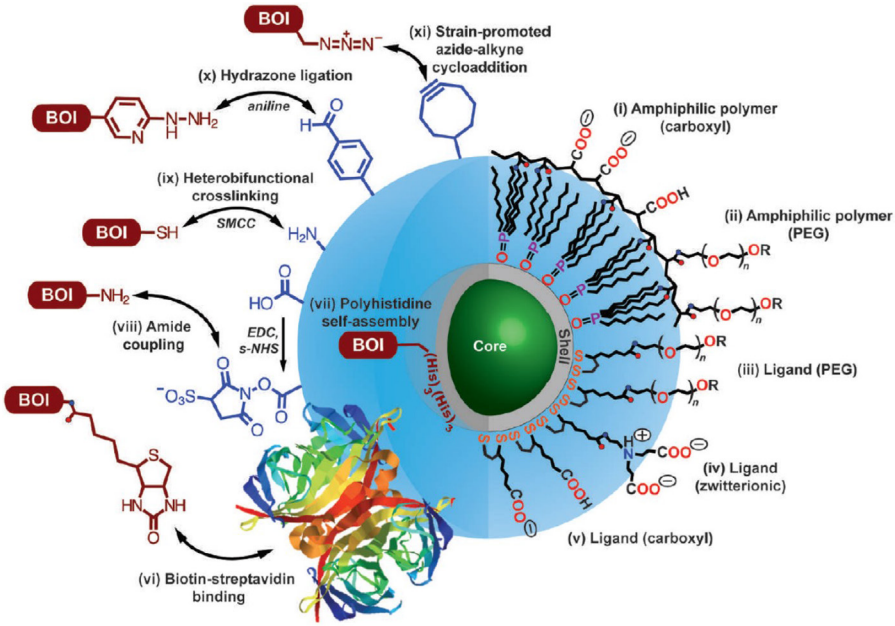


**Fig. 12.2** The various strategies of different bioconjugations with QDs. Right side (surface coating): Hydrophilic ligand exchange and encapsulation with an amphiphilic polymer are two routes for qater-soluble QDs. *Left side* (biomolecules of interest, BOI): the chemical covalent modification offers the possibility to modify with some BOIs (e.g., antibodies or enzymes) [18].

solubility. As illustrated in Fig. 12.2, there are two commonly established routes for water-soluble QDs [15,18]: (I) Ligand exchange and (II) Encapsulation with amphiphilic polymer. (I) An additional surface modification step can be circumvented if the hydrophobic ligands are replaced by hydrophilic ligands as the QDs growth-controlling reagent. Many functional groups are amenable to improving the dispersibility of QDs in water or aqueous buffers such as hydroxyl groups, primary or secondary amines, maleimides, epoxides, carboxylic acids, or phosphonates. Each functionality improves the hydrophilicity to a different extent and especially ionic groups exert a particularly strong influence on the dispersibility. The ligand exchange approach is easy to perform, but the resulting water-soluble QDs are only stable for a short period and its quantum yield decreases significantly. (II) The newly discovered approach is encapsulating QDs by amphiphilic polymers. Typically, amphiphilic polymers contain both a hydrophobic segment or side-chain (mostly hydrocarbons) and a hydrophilic segment or group. The hydrophobic domains strongly interact with QD surface, whereas the hydrophilic groups face outward and render QDs water soluble. In addition, additional functions could be added to QDs through different amphiphilic polymers. For example functional groups at the terminal of amphiphilic zwitterionic-PEG molecules could enable further conjugation of targeting molecules on the surface of the QDs. Zwitterionic moieties could be utilized to reduce nonspecific absorption of proteins on QDs [19].

The larger surface of QDs offers the possibility of binding multiple biomolecules of interest, such as antibodies or some specific functionalized protein, in biomedical applications. Using chemical covalent modification is another strategy for providing a new covalent bond between a biomolecule and the ligand coating on QDs. As previously mentioned, the modification of hydrophilic ligand exchange and encapsulation with an amphiphilic polymer on the outer surface of QDs can provide the hydrophilic property needed to make inorganic QDs soluble in aqueous solutions and in physical environments. After improving the solubility of QDs and versatile chemical modification, both in vitro and in vivo biomedical applications of those water-soluble QDs have made many achievements in imaging and detection.

### 12.1.5 Applications

The water-soluble QDs with the specific optical property are considered as novel materials combining diagnostic purposes for numerous clinical applications. On the other hand, the cytotoxicity of QDs for in vitro and in vivo assay must be considered. Here we review the clinical applications, including (1) QDs conjugated with cancer biomarkers for detection in various cancers and (2) QDs as imaging probes for sensing infectious diseases. The QDs conjugated with cancer biomarkers are detecting tools for diagnosis, forecasting disease stages, and clinical management [20]. The early diagnosis of any type of cancer is important in clinical medicine, and the clinical outcome of a cancer diagnosis is highly dependent on the stage in which the malignancy is detected [21]. Tu et al. demonstrated silicon QD (SiQD) conjugated with an anti-Her2 antibody as a long-lifetime red fluorescence probe (PL spectrum with a single peak at 621 nm under 365 nm excitation) to selectively recognize Her2-overexpressing SKOV3 cells. They also used bovine serum albumin (BSA) and PEG polymers coated on the SiQD surface to form an antifouling layer against the nonspecific absorption of nonexpressing CHO cells. Finally, the in vitro cell viability assay revealed that the $IC_{50}$ is about 1600 $\mu g\,mL^{-1}$ of BSA-terminated SiQDs after 48 h of treatment [22]. In addition, QDs can be designed to be a sensing element for diagnosing infectious diseases such as respiratory syncytial virus (RSV), a virus of the Paramyxoviridae family [23]. Shuming Nie and his group developed the bioconjugated QDs combined with a two-color fluorescence coincidence for real-time detection of the intact RSVs in a flow channel system [24] (Fig. 12.3).

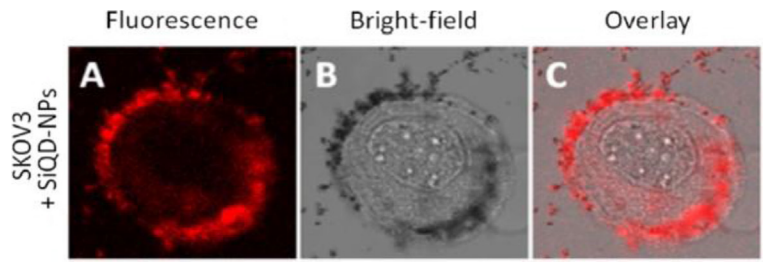


**Fig. 12.3** The confocal fluorescence images of SKOV3 cells treatment with SiQD conjugated with anti-Her2 antibody [22].

Quantum diamond, carbon dot, lanthanide-based upconversion nanoparticles, graphene oxide (GO), and fluorescent dye-doped silica nanoparticles are other fluorescence materials that not only exhibit the specific photophysical property but also provide the possibility of binding antibodies, enzymes, and some functionalized proteins for biomedical diagnosis.

## 12.2 One-dimensional (1-D) nanostructured materials

### *12.2.1 Introduction*

Many scientists have shown interest in 1-D nanostructured materials, and owing to their unique physical properties, they have become the novel materials used in biomedical applications. Wires, rods, belts, and tubes are 1-D nanostructured materials. 1-D nanostructured materials with electrical properties are often fabricated for nanoscale electronic devices used in clinical diagnoses. Here we focus on the wires that we call nanowires (NWs). In a NW, electrons transport along the axis of the NW and then produce an electrical signal when analytes chemically bind or physically absorb along the NW. Among the many types of NWs are elemental semiconductor NWs, metal chalcogenide NWs, and transition-metal NWs. Of these various NWs, we are interested in the silicon NW field-effect transistors (Si-NW FETs), which were first reported in 2001 [25]. Also, they have been developed as a powerful biosensor to measure the receptor-target interaction on the surface of Si-NW FETs, and they can convert the biochemical results to quantifiable electronic signals. We start with a brief introduction about the working principle and measuring concept of Si-NW FETs and then describe the innovative design of subnanostructured Si-NW FETs and their biological and clinical applications [26].

### *12.2.2 The working principle and the sensing mechanism of Si-NW FETs*

A schematic illustration of the working principle and the sensing mechanism of Si-NW FET is shown in Fig. 12.4. A typical Si-NW FET device consists of *p*/*n*-type single-crystalline Si-NWs as the conducting channels, which comprise the source (S), the drain (D), and the gate electrodes. In the Si-NW FET system, the source and the drain electrodes are used to connect silicon nanowire and allow the current on the semiconductor channel to flow from source to drain; the gate electrode modulates the channel conductance via the applied electrical potential [28] and stabilizes the signal by reducing the electron density accumulated in the microfluidic channel [27]. For biological sensing, the biological receptors usually are anchored on the surface of Si-NWs so that the receptors can recognize the target analytes by their highly specific binding affinity. When the receptors capture the targets, the surface potential of the Si-NW changes drastically and induces the channel conductance changes. The conductance changes are recorded and further processed by the electrical measurement

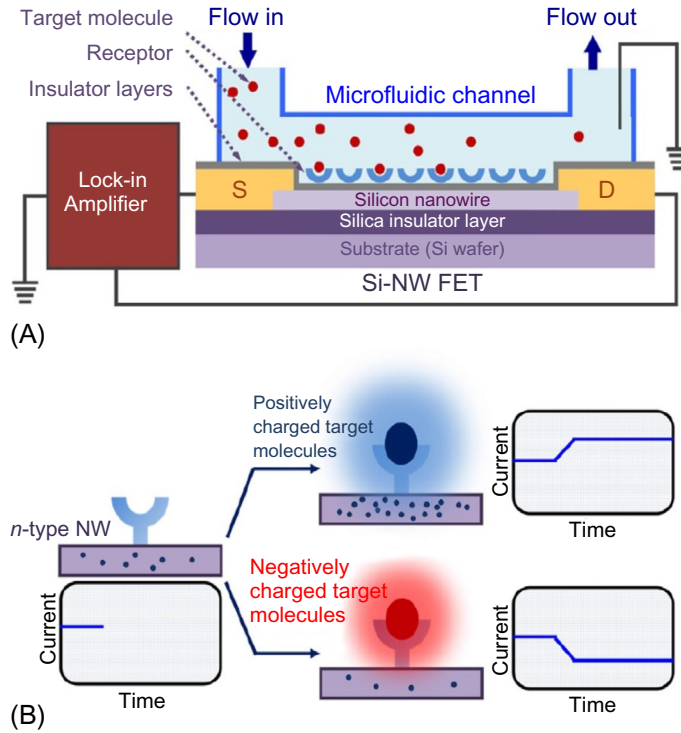


**Fig. 12.4** A schematic illustration of the working principle and the sensing mechanism of Si-NW FET. (A) A Si-NW FET biosensor consists of a single silicon nanowire with the source (S) and drain (D) electrodes placed on a Si wafer. A microfluidic channel is utilized to pretreat the samples. The lock-in amplifier records the electrical signal with a water-gate electrode (e.g., Ag/AgCl reference electrode) in the buffer solution. (B) The biological receptors anchored on the silicon nanowires are utilized to recognize specific target analytes with a Si-NW FET biosensor. The different results of electrical signals rely on positively/negatively charged target molecules [27].

system. For instance, when the negatively charged target molecules bind to the receptors modified on an *n*-type semiconductor channel, the electron carriers are decreased in the semiconductor channel, which reduces the electrical conductance. On the other hand, when positively charged targets are captured by the receptors, the electron carriers increase and thus enhance the electrical conductance.

As for the sensing mechanism of Si-NW FETs, the interaction of biomolecules and Si-NW FETs are expected to induce the conductance changes in the local charges on the surface of Si-NW FETs under the physicochemical environment ($1\times$PBS, 137 mM NaCl, 2.7 mM KCl, 10 mM $Na_2HPO_4$, 2 mM $KH_2PO_4$, pH 7.4). However, a high ionic solution is a crucial factor in weakening the electrical signal in the FET sensing channel. Therefore it is necessary to select the electrolytic buffer solution with an appropriate Debye-Hückel screening length ($\lambda_D$) to reduce the interference in the signal collection [29,30].

### 12.2.3 Innovative design of subnanostructured Si-NW FETs

In the Si-NW FETs, the Si-NWs have large surface-to-volume ratio (SVR), which can enhance the sensitivity of detection. Thus scientists want to fabricate the smaller size of the Si-NWs, down to 20 nm or below. However, because of the limitation of the lithography process, it is difficult to use the top-down methods to reduce the size of Si-NWs. Therefore another feasible approach to enlarge the SVR of the Si-NWs should be considered.

Seol et al. developed an alternative approach to selectively modify the surface of Si-NWs forming the nano-forest structure in top-down fabricated Si-NWs [31]. The formation of the nano-forest structure was achieved by metal-assisted chemical etching. The process was used to remove PMMA on the Si-NWs and then thermally deposit 70 Å gold films on the NWs. Subsequently, the gold film was directly annealed to form the particles. The morphology of the nano-forest significantly enlarged the SVR of the Si-NWs, which improved the sensitivity [31]. As illustrated in Fig. 12.5, we can observe the nano-forest structure forming on the Si-NWs by the localized Joule-heating method and thus enhance the electrical conductance. Other similar approaches

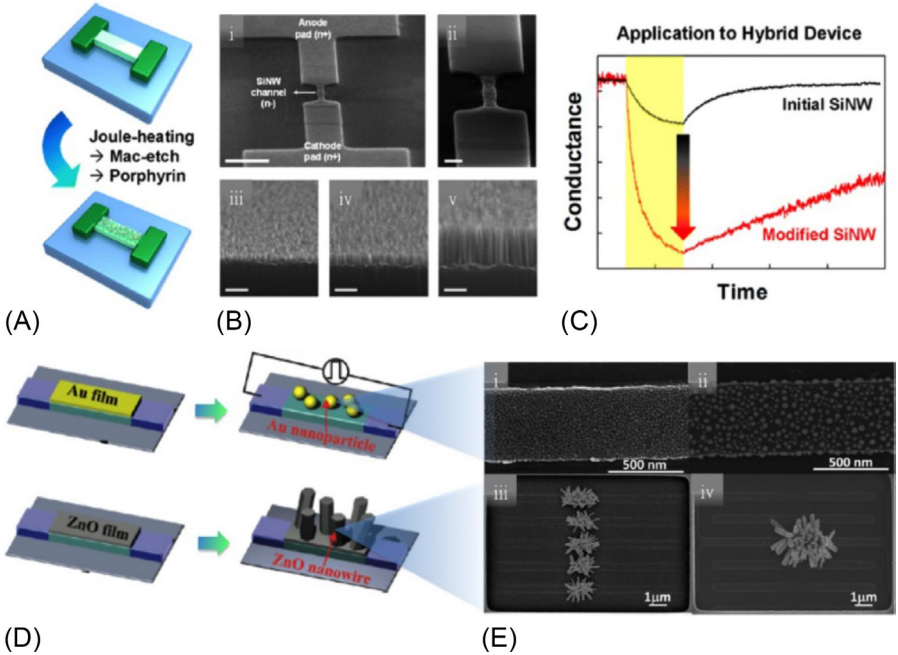


**Fig. 12.5** (A) An illustration of the innovative design of the sub-nanostructured Si-NW FETs: (B) top-view SEM images of nano-forest structure in silicon nanowires; (C) real-time recording of electrical conductance changes on Si-NW FET biosensor with/without nano-forest structure; (D) illustration of growing Au particles or ZnO nanorods on silicon nanowires; (E) SEM images of as-grown Au film (i) and after the localized joule heating (ii), and SEM images of ZnO nanorods selectively grown on multiple (iii) and single (iv) silicon nanowires [27].

were reported to choose Au particles or ZnO nanorods grown on the Si-NWs to increase the SVR (Fig. 12.5) [32].

### 12.2.4 The biological and clinical applications

In biological sensing, Si-NW FETs exhibit their potential applications, which include detecting protein-protein interactions, monitoring the release of neurotransmitters, probing small biomolecules, and aiding clinical diagnoses. Unlike the traditional optical or electrochemical biosensors, Si-NW FETs not only have time-saving procedures but also display high-sensitivity detection and selectivity of specific targets. Using label-free assays involving real-time recording is another advantage of Si-NW FETs.

### 12.2.5 Protein-protein interaction

In order to discover how proteins recognize other proteins, Si-NW FETs are used to explore the interaction between two proteins in a physicochemical environment. A rapid and reliable device is important for this purpose. For example, Cui et al. reported the real-time detection of streptavidin with a biotin-modified Si-NW FET biosensor. Lin et al. first demonstrated a Si-NW FET biosensor for rapid measuring of protein-protein interactions [33]. They used glutathione *S*-transferase (GST)-fused CaM (called CaM-GST) on a glutathione (GSH)-modified Si-NW FET to examine the protein-protein interaction caused by the reversible association of GSH-GST.

### 12.2.6 Probing the small biomolecules

Probing the small biomolecules is a potential application for biological and clinical research. However, a major challenge is lower sensitivity for the small biomolecules. Thus Si-NW FETs is a great candidate for probing the small biomolecules because the electrical signals are much more sensitive than the signals of the optical or electrochemical biosensors. Li et al. demonstrated an ultrasensitive Si-NW FET biosensor to selectively probe dopamine, an important neurotransmitter [34]. The detection limit is about $10^{-11}$ M. They used the specific aptamer modified on multiple-parallel-connected Si-NWs to monitor dopamine release under hypoxic stimulation from living PC12 cells. Moreover, the aptamer-based Si-NW FET biosensor displayed a high specific binding affinity to dopamine.

### 12.2.7 Clinical diagnosis

Early diagnosis of disease pathogenesis is critical in the detection of biomarkers because of the extremely low concentration of target species and possible interference existing in the complicated physiological samples. Si-NW FET biosensors can provide highly sensitive, label-free, and real-time detection of biomarkers.

Si-NE FET biosensors have demonstrated success for several applications in disease identification. For instance, cardiac troponin I, one kind of biomarker, has high sensitivity and specificity for detecting acute myocardial infarction [35].

The Si-NW FET biosensor, which immobilized with anticardiac troponin I antibody, displays an excellent detection limit of 0.092 ng $L^{-1}$ with a wide linear range of 0.0092–46 ng $mL^{-1}$ for cardiac troponin I [36]. Also, a Si-NW FET biosensor can be fabricated in an array-structured device to achieve multiple detection of cancer biomarkers. For example, antibodies of three different cancer biomarkers (prostate-specific antigen, carcinoembryonic antigen, and mucin-1) were individually modified on three different Si-NW FET units in an array. This system displayed high-detection selectivity and simultaneous recording of each Si-NW FET unit for three different biomarkers with a detection limit down to 0.9 pg $mL^{-1}$ in undiluted serum samples [37].

## 12.3 Two-dimensional (2-D) nanostructured materials

### *12.3.1 Introduction*

GO is a derivative of graphene and consists of a single-layer GO usually produced by the chemical treatment of graphite through oxidation. The oxygen-containing functional group has been well studied. These studies revealed the oxygen functional group mainly forming the hydroxyl and epoxy groups on the basal plane, and smaller amounts of carboxy, carbonyl, phenol, lactone, and quinone at the sheet edges [38–40]. In addition, GO displayed good biocompatibility and is a promising material for biomedical applications. GO has attracted enormous interest in the fields of bioimaging, biosensors, and bioassays because of its excellent aqueous processability, amphiphilicity, surface functionalizability, and surface-enhanced Raman scattering (SERS) property [41].

### *12.3.2 Synthesis of GO*

The synthesis method for GO is either chemical or thermal reduction processes. Among the various synthesis methods, the most important and widely used one was developed by Hummers and Offeman in 1958 (Hummers' method) [42]. This method used oxidation of graphite with harsh treatment of one equal weight of graphite powder in a concentrated $H_2SO_4$ solution containing three equal weights of $KMnO_4$ and 0.5 equal weight of $NaNO_3$. Then the GO was chemically exfoliated from an oxidized graphite solution with sonication. The chemical structure of GO is shown in Fig. 12.6 [43]. Although the Hummers' method is an efficient and much safer method for synthesizing GO, it may bring some harmful and toxic species, which are considered. The drawbacks of the Hummers' method are as follows: (1) the oxidation procedure releases toxic gasses such as $NO_2$ and $N_2O_4$; (2) the residual $Na^+$ and $NO_3^-$ ions are difficult to remove from the waste water formed from the processes of synthesizing and purifying GO [44]. Chen et al. synthesized GO using an improved Hummers' method without utilizing $NaNO_3$ [44], which is an eco-friendly way to produce GO.

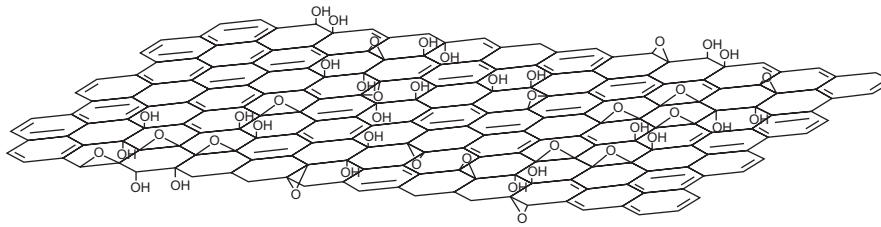

**Fig. 12.6** The chemical structure of graphene oxide [43].

### 12.3.3 Structure of GO

The precise atomic structure of GO is still uncertain, and no powerful analytic technique for characterizing the real structure of GO exists currently. Scientists have surveyed and tried to explore the atomic details of the GO structure in depth. In 2006 Szabó et al. [45] proposed a new model involving a carbon network comprising two kinds of regions: (1) translinked cyclohexane chairs and (2) ribbons of flat hexagons with carbon-carbon double bonds with functional groups such as tertiary OH, 1,3-ether, ketone, quinone, and phenol (aromatic diol). A single-layer GO consists of a hexagonal ring-based carbon network involving both $sp^2$-hybridized carbon atoms (largely) and $sp^3$-hybridized carbons bearing oxygen functional groups (partly) [45,46]. To explore the GO structure much more deeply, some microscopic and spectroscopic techniques have been considered to precisely characterize its structural features. Atomic force microscope, for example, is employed to reveal directly the thickness of a single-layer GO and the number of layers. Moreover, high-resolution transmission electron microscopy is utilized to directly observe imaging of lattice atoms and topological defects in a single-layer GO. On the other hand, using various spectroscopic techniques can identify the chemical composition of GO and the amount of oxygen groups in GO. These spectroscopic techniques include solid-state nuclear magnetic resonance (SSNMR), X-ray photoelectron spectroscopy (XPS), Raman spectroscopy, and Fourier transform infrared spectroscopy (FT-IR). The typical SSNMR can identify the degree of bond hybridization in mixed $sp^2/sp^3$ bonded carbon and the specific bonding configurations of functional atoms. There are three main peaks in the $^{13}C$ NMR spectrum. A peak of about 60 ppm is ascribed to carbon atoms bonding to the epoxy group, the peak around 70 ppm is assigned to the hydroxyl group connected to the carbon atoms, and the peak around 130 ppm corresponds to the graphitic $sp^2$ carbon. Also, XPS reveals the various states of specific atom bonds in one kind of materials. We can observe the different photon energy of the carbon and oxygen bonds to identify the atomic states of GO. FT-IR spectroscopy is a powerful tool for identifying the functional groups of the materials. In GO, it involves hydroxyl (broad peak at 3050–3800 $cm^{-1}$), carbonyl (1750–1850 $cm^{-1}$), carboxyl (1650–1750 $cm^{-1}$), carbon double bond (1500–1600 $cm^{-1}$), and ether or epoxide (1000–1280 $cm^{-1}$) groups. Conversely, theoretical researches are expected to explore the more detailed information about the complex structure of GO.

## 12.3.4 Application

### 12.3.4.1 GO FRET sensing system

GO has been used as a sensing platform to probe some biomolecules and harmful metal ions. This work involves using aptamer probes with fluorescence dye to observe the fluorescence changes by fluorescence resonance energy transfer (FRET) between the fluorescence dye-modified aptamer and GO. Wang et al. developed an aptamer-based GO platform to probe molecules in living cells [47]. The schematic illustration of probing molecules in living cells by an aptamer-based GO platform is shown in Fig. 12.7. They used an ATP aptamer with fluorophore carboxyfluorescein (FAM), which was modified on the GO to form aptamer-FAM/GO. After a few minutes, the fluorescence was quenched with very fast kinetics because of the FRET between FAM and GO [48,49]. While the ATP solution was injected into the ATP aptamer-FAM/GO system, they observed the obvious fluorescence recovery because the ATP aptamer could probe ATP and then form the duplex configuration, which would be released from the surface of GO. This system also displayed its high sensitivity and a wide detecting range, from 10 µm to 2.5 mM, for in vitro. Also, it had high selectivity only for ATP and its fluorescence recovery up to 85.7%; neither CTP, TTP, nor CTP was observed with any fluorescence recovery. To enhance the efficiency of the GO FRET sensing system, it is important to understand the chemical/physical-related mechanism of the molecule and GO platform.

### 12.3.4.2 Cell capturing

Capturing circulating tumor cells (CTCs) in blood is a widespread topic in clinical research, including for metastatic breast, prostate, colorectal, and lung cancer. An accurate quantification of CTCs in the bloodstream is very important and is a crucial factor for the overall survival of cancer patients. CTCs are extremely rare epithelial cells (1–10 cells/mL) present in patients' blood, so it is challenging to capture CTCs in the bloodstream. GO offers an opportunity to capture CTCs. Because the size of CTCs is larger than the pore size of GO, GO cannot be used to filter and capture CTCs from blood samples. Nellore et al. demonstrate an aptamer-conjugated GO membrane to capture the multiple types of CTCs [50]. This membrane can capture SKBR3 breast cancer cells, LNCaP prostate cancer cells, and SW-948 colon cancer cells selectively and simultaneously from infected blood. It has a 98% capture efficiency. At the same

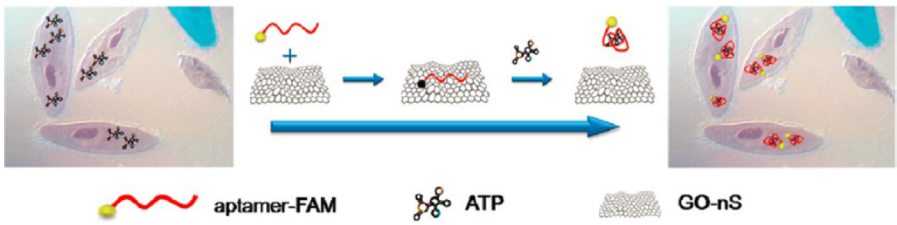


**Fig. 12.7** The schematic illustration of an aptamer-based GO platform for probing biomolecules in living cells [47].

time, capturing a specific white blood cell (WBC) has attracted enormous interest for biomedical applications. For instance, Chen et al. developed quick and highly efficient GO nanosheets to capture distinct WBC subpopulations from small samples (~30 mL) of whole blood [51]. They modified some single-domain antibodies (e.g., VHH7 and VHH DC13) on the GO. These functionalized surfaces can then selectively capture Class II MHC-positive ($MHC^+$) and CD11b-positive ($CD11b^+$) cells from small volumes (~30 mL) because GO nanosheets possess good biocompatibility, large surface area, good water dispersibility, and ease of facial surface modification. The GO nanosheets are expected to be the promising materials for capturing specific cells in whole blood.

#### *12.3.4.3 Tumor diagnosis*

Malignant tumors are the leading cause of death in humans. The tumor imaging probes, which consist of one fluorescence dye and one tumor target, are expected to be useful tools in diagnosing tumors in vivo or in vitro. However, these "always-on" probes are associated with high background fluorescence and insufficient sensitivity to detect small numbers of malignant tumor cells. Therefore an ideal tumor imaging probe should be "switched on"; that is, a signal is triggered while the tumor target recognizes the tumor cells. In 2013 Yue et al. developed an inducible GO probe for early tumor diagnosis [52]. In this system, the Cy5 fluorescence molecule was modified on GO through the specific peptide (Gly-Pro-Leu-Gly-Val-Arg-Gly-Cys). Cy5 fluorescence was quenched because of its proximity to GO, but triggered and then switched on once the specific regions on the tumor cells were probed (Fig. 12.8). Moreover, this system can be applied to monitor tumor invasiveness and metastasis, and it is able to contour the tumor shape in clinical diagnosis and surgery therapy.

### *12.3.5 Three-dimensional (3-D) nanostructured materials*

In the last part of this chapter, we briefly introduce three-dimensional materials used for numerous clinical applications. In the last 20 years, the metal nanoclusters (<2 nm) (e.g., Au, Ag, Pt, and Cu) consisting of several to a few hundred atoms have become a new kind of material with outstanding chemical and physical properties [53]. The metal nanoclusters exhibit molecule-like characteristics as their size approaches the

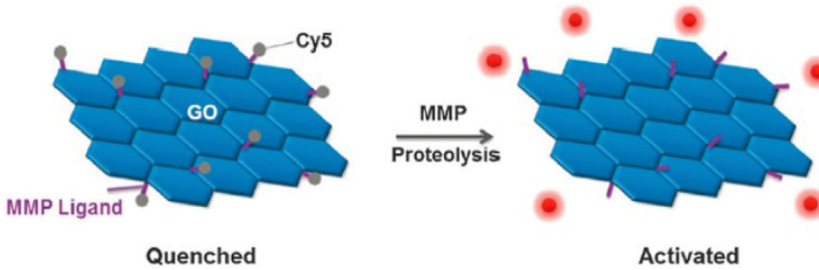


**Fig. 12.8** The strategy and principle of an inducible GO probe for specific tumor imaging [52].

Fermi wavelength of electrons, which produce the unique electrical, chemical, and optical properties, including good quantum yield, large Stock shift, high photostability, and tunable fluorescence [54–57]. Because of their excellent features, meal nanoclusters have attracted a good deal of attention in regard to biological and medical applications, such as nucleic acid detection for diagnosis of some diseases [58–62], microRNA detection for early diagnosis of disease and study of new anticancer drugs [63–66], detection of small biomolecules [67–70] (e.g., urea, dopamine, glucose, reactive oxygen species, theophylline, and biological thiols), and in vitro and in vivo bioimaging for targeting tumor cells [71–77].

## 12.4 Summary

Finally, we summarize Table 12.2 of the nanostructured materials, which are classified in four groups by dimensions, that is, from zero to three dimensions. These inorganic materials' surfaces usually need to be modified with linkers, which can improve the

**Table 12.2 Summary of nanostructured materials in medical diagnosis**

| Dimension | Materials | Detection type | Application | References |
|---|---|---|---|---|
| Zero-dimension | Quantum Dots | Fluorescence imaging | Detection of cancer or tumor cells | [22,78–84] |
| | | Fluorescence signal | Sensing of infectious diseases | [24,85] |
| One-dimension | SiNW-FET | Electrical signal | Virus detection | [86,87] |
| | | | Small biomolecule detection | [34,88,89] |
| | | | DNA/RNA detection | [90–92] |
| Two-dimension | Graphene oxide | Fluorescence signal | Sensitive capture of cells | [50,51,93] |
| | | Electrical signal | Diagnosis of cancer biomarker | [94–96] |
| Three-dimension | Metal nanoclusters | Fluorescence signal | Diagnosis of some diseases | [54–57,97] |
| | | | Small biomolecules detection | [67–70,98–100] |
| | | | Bioimaging for targeting tumor cells | [71–77,101–103] |

materials' water solubility and enable binding of biomolecules (e.g., antibodies, enzymes) for medical diagnosis. QDs exhibit unique photophysical properties, including multiple emission spectra, good quantum yield, and photostability because of the quantum confinement. Medical applications of QDs center on bioimaging probes for the detection of certain cancer and tumor cells. We can observe the fluorescence images of cancer or tumor cells because QDs conjugated with biomarkers can recognize specific targets on the surface of cancer and tumor cells. The Si-NW FET biosensor produces an electrical signal because the receptor recognizes the target and then changes the charge density of the Si-NW, inducing the change of electrical conductance. The Si-NW FET provides a high sensitivity and selectivity, label-free, and real-time detection platform for various clinical diagnoses of diseases. Because of their excellent aqueous processability, amphiphilicity, surface functionalizability, and SERS property, GOs are the novel material attracting significant attention in the biosensing fields. GOs can be a platform to CTCs for early diagnosis of cancer cells. Metal nanoclusters display good quantum yield, large Stock shift, high photostability, and tunable fluorescence, making them an alternative fluorescence probe for versatile biomedical applications.

## References

[1] D. Bera, L. Qian, T.-K. Tseng, P.H. Holloway, Quantum dots and their multimodal applications: a review, Materials 3 (4) (2010) 2260.
[2] J. Bang, H. Yang, P.H. Holloway, Enhanced and stable green emission of ZnO nanoparticles by surface segregation of Mg, Nanotechnology 17 (4) (2006) 973.
[3] L. Spanhel, M.A. Anderson, Semiconductor clusters in the sol-gel process: quantized aggregation, gelation, and crystal growth in concentrated zinc oxide colloids, J. Am. Chem. Soc. 113 (8) (1991) 2826.
[4] D. Bera, L. Qian, S. Sabui, S. Santra, P.H. Holloway, Photoluminescence of ZnO quantum dots produced by a sol-gel process, Opt. Mater. 30 (8) (2008) 1233.
[5] L. Qu, X. Peng, Control of photoluminescence properties of CdSe nanocrystals in growth, J. Am. Chem. Soc. 124 (9) (2002) 2049.
[6] C. Murray, D.J. Norris, M.G. Bawendi, Synthesis and characterization of nearly monodisperse CdE (E=sulfur, selenium, tellurium) semiconductor nanocrystallites, J. Am. Chem. Soc. 115 (19) (1993) 8706.
[7] L. Qu, Z.A. Peng, X. Peng, Alternative routes toward high quality CdSe nanocrystals, Nano Lett. 1 (6) (2001) 333.
[8] L. Li, H. Qian, J. Ren, Rapid synthesis of highly luminescent CdTe nanocrystals in the aqueous phase by microwave irradiation with controllable temperature, Chem. Commun. 4 (2005) 528.
[9] M.T. Swihart, Vapor-phase synthesis of nanoparticles, Curr. Opin. Colloid Interface Sci. 8 (1) (2003) 127.
[10] K. Leonardi, H. Selke, H. Heinke, K. Ohkawa, D. Hommel, F. Gindele, U. Woggon, Formation of self-assembling II–VI semiconductor nanostructures during migration enhanced epitaxy, J. Cryst. Growth 184 (1998) 259.
[11] E. Kurtz, J. Shen, M. Schmidt, M. Grün, S. Hong, D. Litvinov, D. Gerthsen, T. Oka, T. Yao, C. Klingshirn, Formation and properties of self-organized II–VI quantum islands, Thin Solid Films 367 (1) (2000) 68.

[12] J. Li, J.-J. Zhu, Quantum dots for fluorescent biosensing and bio-imaging applications, Analyst 138 (9) (2013) 2506.
[13] W.C. Chan, D.J. Maxwell, X. Gao, R.E. Bailey, M. Han, S. Nie, Luminescent quantum dots for multiplexed biological detection and imaging, Curr. Opin. Biotechnol. 13 (1) (2002) 40.
[14] W.R. Algar, K. Susumu, J.B. Delehanty, I.L. Medintz, Semiconductor quantum dots in bioanalysis: crossing the valley of death, Anal. Chem. 83 (23) (2011) 8826.
[15] K.D. Wegner, N. Hildebrandt, Quantum dots: bright and versatile in vitro and in vivo fluorescence imaging biosensors, Chem. Soc. Rev. 44 (14) (2015) 4792.
[16] A.M. Smith, S. Nie, Semiconductor nanocrystals: structure, properties, and band gap engineering, Acc. Chem. Res. 43 (2) (2009) 190.
[17] I.L. Medintz, H.T. Uyeda, E.R. Goldman, H. Mattoussi, Quantum dot bioconjugates for imaging, labelling and sensing, Nat. Mater. 4 (6) (2005) 435.
[18] E. Petryayeva, W.R. Algar, I.L. Medintz, Quantum dots in bioanalysis: a review of applications across various platforms for fluorescence spectroscopy and imaging, Appl. Spectrosc. 67 (3) (2013) 215.
[19] E.L. Bentzen, I.D. Tomlinson, J. Mason, P. Gresch, M.R. Warnement, D. Wright, E. Sanders-Bush, R. Blakely, S.J. Rosenthal, Surface modification to reduce nonspecific binding of quantum dots in live cell assays, Bioconjug. Chem. 16 (6) (2005) 1488.
[20] K.H. Lee, J.F. Galloway, J. Park, C.M. Dvoracek, M. Dallas, K. Konstantopoulos, A. Maitra, P.C. Searson, Quantitative molecular profiling of biomarkers for pancreatic cancer with functionalized quantum dots, Nnomed. Nanotechnol. Biol. Med. 8 (7) (2012) 1043.
[21] A. Gokarna, L.H. Jin, J.S. Hwang, Y.H. Cho, Y.T. Lim, B.H. Chung, S.H. Youn, D.S. Choi, J.H. Lim, Quantum dot-based protein micro-and nanoarrays for detection of prostate cancer biomarkers, Proteomics 8 (9) (2008) 1809.
[22] C.-C. Tu, K.-P. Chen, T.-A. Yang, M.-Y. Chou, L.Y. Lin, Y.-K. Li, Silicon quantum dot nanoparticles with antifouling coatings for immunostaining on live cancer cells, ACS Appl. Mater. Interfaces 8 (22) (2016) 13714.
[23] P. Tallury, A. Malhotra, L.M. Byrne, S. Santra, Nanobioimaging and sensing of infectious diseases, Adv. Drug Deliv. Rev. 62 (4) (2010) 424.
[24] A. Agrawal, C. Zhang, T. Byassee, R.A. Tripp, S. Nie, Counting single native biomolecules and intact viruses with color-coded nanoparticles, Anal. Chem. 78 (4) (2006) 1061.
[25] Y. Cui, Q. Wei, H. Park, C.M. Lieber, Nanowire nanosensors for highly sensitive and selective detection of biological and chemical species, Science 293 (5533) (2001) 1289.
[26] A. Zhang, C.M. Lieber, Nano-bioelectronics, Chem. Rev. 116 (1) (2015) 215.
[27] M.-Y. Shen, B.-R. Li, Y.-K. Li, Silicon nanowire field-effect-transistor based biosensors: from sensitive to ultra-sensitive, Biosens. Bioelectron. 60 (2014) 101.
[28] B.-R. Li, C.-C. Chen, U.R. Kumar, Y.-T. Chen, Advances in nanowire transistors for biological analysis and cellular investigation, Analyst 139 (7) (2014) 1589.
[29] A. Vacic, J.M. Criscione, N.K. Rajan, E. Stern, T.M. Fahmy, M.A. Reed, Determination of molecular configuration by Debye length modulation, J. Am. Chem. Soc. 133 (35) (2011) 13886.
[30] E. Stern, J.F. Klemic, D.A. Routenberg, P.N. Wyrembak, D.B. Turner-Evans, A.D. Hamilton, D.A. LaVan, T.M. Fahmy, M.A. Reed, Label-free immunodetection with CMOS-compatible semiconducting nanowires, Nature 445 (7127) (2007) 519.
[31] M.-L. Seol, J.-H. Ahn, J.-M. Choi, S.-J. Choi, Y.-K. Choi, Self-aligned nanoforest in silicon nanowire for sensitive conductance modulation, Nano Lett. 12 (11) (2012) 5603.

[32] K.-I. Chen, B.-R. Li, Y.-T. Chen, Silicon nanowire field-effect transistor-based biosensors for biomedical diagnosis and cellular recording investigation, Nano Today 6 (2) (2011) 131.
[33] T.-W. Lin, P.-J. Hsieh, C.-L. Lin, Y.-Y. Fang, J.-X. Yang, C.-C. Tsai, P.-L. Chiang, C.-Y. Pan, Y.-T. Chen, Label-free detection of protein-protein interactions using a calmodulin-modified nanowire transistor, Proc. Natl. Acad. Sci. 107 (3) (2010) 1047.
[34] B.-R. Li, Y.-J. Hsieh, Y.-X. Chen, Y.-T. Chung, C.-Y. Pan, Y.-T. Chen, An ultrasensitive nanowire-transistor biosensor for detecting dopamine release from living PC12 cells under hypoxic stimulation, J. Am. Chem. Soc. 135 (43) (2013) 16034.
[35] W. Shen, D. Tian, H. Cui, D. Yang, Z. Bian, Nanoparticle-based electrochemiluminescence immunosensor with enhanced sensitivity for cardiac troponin I using *N*-(aminobutyl)-*N*-(ethylisoluminol)-functionalized gold nanoparticles as labels, Biosens. Bioelectron. 27 (1) (2011) 18.
[36] T. Kong, R. Su, B. Zhang, Q. Zhang, G. Cheng, CMOS-compatible, label-free silicon-nanowire biosensors to detect cardiac troponin I for acute myocardial infarction diagnosis, Biosens. Bioelectron. 34 (1) (2012) 267.
[37] G. Zheng, F. Patolsky, Y. Cui, W.U. Wang, C.M. Lieber, Multiplexed electrical detection of cancer markers with nanowire sensor arrays, Nat. Biotechnol. 23 (10) (2005) 1294.
[38] G. Eda, M. Chhowalla, Chemically derived graphene oxide: towards large-area thin-film electronics and optoelectronics, Adv. Mater. 22 (22) (2010) 2392.
[39] X. Li, G. Zhang, X. Bai, X. Sun, X. Wang, E. Wang, H. Dai, Highly conducting graphene sheets and Langmuir-Blodgett films, Nat. Nanotechnol. 3 (9) (2008) 538.
[40] F. Kim, L.J. Cote, J. Huang, Graphene oxide: surface activity and two-dimensional assembly, Adv. Mater. 22 (17) (2010) 1954.
[41] C. Chung, Y.-K. Kim, D. Shin, S.-R. Ryoo, B.H. Hong, D.-H. Min, Biomedical applications of graphene and graphene oxide, Acc. Chem. Res. 46 (10) (2013) 2211.
[42] W.S. Hummers, R.E. Offeman, Preparation of graphitic oxide, J. Am. Chem. Soc. 80 (6) (1958) 1339.
[43] D.A. Dikin, S. Stankovich, E.J. Zimney, R.D. Piner, G.H. Dommett, G. Evmenenko, S.T. Nguyen, R.S. Ruoff, Preparation and characterization of graphene oxide paper, Nature 448 (7152) (2007) 457.
[44] J. Chen, B. Yao, C. Li, G. Shi, An improved Hummers method for eco-friendly synthesis of graphene oxide, Carbon 64 (2013) 225.
[45] T. Szabó, O. Berkesi, P. Forgó, K. Josepovits, Y. Sanakis, D. Petridis, I. Dékány, Evolution of surface functional groups in a series of progressively oxidized graphite oxides, Chem. Mater. 18 (11) (2006) 2740.
[46] T. Nakajima, Y. Matsuo, Formation process and structure of graphite oxide, Carbon 32 (3) (1994) 469.
[47] Y. Wang, Z. Li, D. Hu, C.-T. Lin, J. Li, Y. Lin, Aptamer/graphene oxide nanocomplex for in situ molecular probing in living cells, J. Am. Chem. Soc. 132 (27) (2010) 9274.
[48] C.-H. Lu, H.-H. Yang, C.-L. Zhu, X. Chen, G.-N. Chen, A graphene platform for sensing biomolecules, Angew. Chem. Int. Ed. 48 (26) (2009) 4785.
[49] Z. Tang, H. Wu, J.R. Cort, G.W. Buchko, Y. Zhang, Y. Shao, I.A. Aksay, J. Liu, Y. Lin, Constraint of DNA on functionalized graphene improves its biostability and specificity, Small 6 (11) (2010) 1205.
[50] B.P. Viraka Nellore, R. Kanchanapally, A. Pramanik, S.S. Sinha, S.R. Chavva, A. Hamme, P.C. Ray, Aptamer-conjugated graphene oxide membranes for highly efficient capture and accurate identification of multiple types of circulating tumor cells, Bioconjug. Chem. 26 (2) (2015) 235.

[51] G.-Y. Chen, Z. Li, C.S. Theile, N.M. Bardhan, P.V. Kumar, J.N. Duarte, T. Maruyama, A. Rashidfarrokh, A.M. Belcher, H.L. Ploegh, Graphene oxide nanosheets modified with single-domain antibodies for rapid and efficient capture of cells, Chem. Eur. J. 21 (48) (2015) 17178.
[52] Z. Yue, P. Lv, H. Yue, Y. Gao, D. Ma, W. Wei, G. Ma, Inducible graphene oxide probe for high-specific tumor diagnosis, Chem. Commun. 49 (37) (2013) 3902.
[53] Y. Tao, M. Li, J. Ren, X. Qu, Metal nanoclusters: novel probes for diagnostic and therapeutic applications, Chem. Soc. Rev. 44 (23) (2015) 8636.
[54] Y. Negishi, K. Nobusada, T. Tsukuda, Glutathione-protected gold clusters revisited: bridging the gap between gold (I)-thiolate complexes and thiolate-protected gold nanocrystals, J. Am. Chem. Soc. 127 (14) (2005) 5261.
[55] J.T. Petty, J. Zheng, N.V. Hud, R.M. Dickson, DNA-templated Ag nanocluster formation, J. Am. Chem. Soc. 126 (16) (2004) 5207.
[56] C.M. Ritchie, K.R. Johnsen, J.R. Kiser, Y. Antoku, R.M. Dickson, J.T. Petty, Ag nanocluster formation using a cytosine oligonucleotide template, J. Phys. Chem. C 111 (1) (2007) 175.
[57] J. Sharma, H.-C. Yeh, H. Yoo, J.H. Werner, J.S. Martinez, A complementary palette of fluorescent silver nanoclusters, Chem. Commun. 46 (19) (2010) 3280.
[58] Y. Xiao, Z. Wu, K.-Y. Wong, Z. Liu, Hairpin DNA probes based on target-induced in situ generation of luminescent silver nanoclusters, Chem. Commun. 50 (37) (2014) 4849.
[59] Y. Zhang, C. Zhu, L. Zhang, C. Tan, J. Yang, B. Chen, L. Wang, H. Zhang, DNA-templated silver nanoclusters for multiplexed fluorescent DNA detection, Small 11 (12) (2015) 1385.
[60] L. Liu, Q. Yang, J. Lei, N. Xu, H. Ju, DNA-regulated silver nanoclusters for label-free ratiometric fluorescence detection of DNA, Chem. Commun. 50 (89) (2014) 13698.
[61] N. Enkin, F. Wang, E. Sharon, H.B. Albada, I. Willner, Multiplexed analysis of genes using nucleic acid-stabilized silver-nanocluster quantum dots, ACS Nano 8 (11) (2014) 11666.
[62] L. Zhang, J. Zhu, S. Guo, T. Li, J. Li, E. Wang, Photoinduced electron transfer of DNA/Ag nanoclusters modulated by G-quadruplex/hemin complex for the construction of versatile biosensors, J. Am. Chem. Soc. 135 (7) (2013) 2403.
[63] S.W. Yang, T. Vosch, Rapid detection of microRNA by a silver nanocluster DNA probe, Anal. Chem. 83 (18) (2011) 6935.
[64] Y.-Q. Liu, M. Zhang, B.-C. Yin, B.-C. Ye, Attomolar ultrasensitive microRNA detection by DNA-scaffolded silver-nanocluster probe based on isothermal amplification, Anal. Chem. 84 (12) (2012) 5165.
[65] P. Shah, A. Rørvig-Lund, S.B. Chaabane, P.W. Thulstrup, H.G. Kjaergaard, E. Fron, J. Hofkens, S.W. Yang, T. Vosch, Design aspects of bright red emissive silver nanoclusters/DNA probes for microRNA detection, ACS Nano 6 (10) (2012) 8803.
[66] X. Qiu, P. Wang, Z. Cao, Hybridization chain reaction modulated DNA-hosted silver nanoclusters for fluorescent identification of single nucleotide polymorphisms in the let-7 miRNA family, Biosens. Bioelectron. 60 (2014) 351.
[67] L.V. Nair, D.S. Philips, R.S. Jayasree, A. Ajayaghosh, A near-infrared fluorescent nanosensor (AuC@ Urease) for the selective detection of blood urea, Small 9 (16) (2013) 2673.
[68] Y. Tao, Y. Lin, J. Ren, X. Qu, A dual fluorometric and colorimetric sensor for dopamine based on BSA-stabilized Aunanoclusters, Biosens. Bioelectron. 42 (2013) 41.
[69] X. Yuan, Y. Tay, X. Dou, Z. Luo, D.T. Leong, J. Xie, Glutathione-protected silver nanoclusters as cysteine-selective fluorometric and colorimetric probe, Anal. Chem. 85 (3) (2013) 1913.

[70] T. Chen, Y. Hu, Y. Cen, X. Chu, Y. Lu, A dual-emission fluorescent nanocomplex of gold-cluster-decorated silica particles for live cell imaging of highly reactive oxygen species, J. Am. Chem. Soc. 135 (31) (2013) 11595.
[71] J. Li, X. Zhong, F. Cheng, J.-R. Zhang, L.-P. Jiang, J.-J. Zhu, One-pot synthesis of aptamer-functionalized silver nanoclusters for cell-type-specific imaging, Anal. Chem. 84 (9) (2012) 4140.
[72] Z. Sun, Y. Wang, Y. Wei, R. Liu, H. Zhu, Y. Cui, Y. Zhao, X. Gao, Ag cluster-aptamer hybrid: specifically marking the nucleus of live cells, Chem. Commun. 47 (43) (2011) 11960.
[73] J. Yin, X. He, K. Wang, Z. Qing, X. Wu, H. Shi, X. Yang, One-step engineering of silver nanoclusters-aptamer assemblies as luminescent labels to target tumor cells, Nanoscale 4 (1) (2012) 110.
[74] J. Liu, M. Yu, X. Ning, C. Zhou, S. Yang, J. Zheng, PE gylation and zwitterionization: pros and cons in the renal clearance and tumor targeting of near-IR-emitting gold nanoparticles, Angew. Chem. Int. Ed. 52 (48) (2013) 12572.
[75] X.-D. Zhang, D. Wu, X. Shen, P.-X. Liu, F.-Y. Fan, S.-J. Fan, In vivo renal clearance, biodistribution, toxicity of gold nanoclusters, Biomaterials 33 (18) (2012) 4628.
[76] P. Zhang, X.X. Yang, Y. Wang, N.W. Zhao, C.Z. Huang, Rapid synthesis of highly luminescent and stable Au 20 nanoclusters for active tumor-targeted imaging in vitro and in vivo, Nanoscale 6 (4) (2014) 2261.
[77] X. Wu, C. Li, S. Liao, L. Li, T. Wang, Z. Su, C. Wang, J. Zhao, C. Sui, J. Lin, Silica-encapsulated $Gd^{3}$+-aggregated gold nanoclusters for in vitro and in vivo multimodal cancer imaging, Chem. A Eur. J. 20 (29) (2014) 8876.
[78] P. Zrazhevskiy, X. Gao, Quantum dot imaging platform for single-cell molecular profiling, Nat. Commun. 2013 (1619) 4.
[79] F. Erogbogbo, K.-T. Yong, R. Hu, W.-C. Law, H. Ding, C.-W. Chang, P.N. Prasad, M.T. Swihart, Biocompatible magnetofluorescent probes: luminescent silicon quantum dots coupled with superparamagnetic iron (III) oxide, ACS Nano 4 (9) (2010) 5131.
[80] L. Shang, R.M. Dörlich, S. Brandholt, R. Schneider, V. Trouillet, M. Bruns, D. Gerthsen, G.U. Nienhaus, Facile preparation of water-soluble fluorescent gold nanoclusters for cellular imaging applications, Nanoscale 3 (5) (2011) 2009.
[81] J. Yu, S. Choi, R.M. Dickson, Shuttle-based fluorogenic silver-cluster biolabels, Angew. Chem. 121 (2) (2009) 324.
[82] J. Gao, K. Chen, R. Xie, J. Xie, S. Lee, Z. Cheng, X. Peng, X. Chen, Ultrasmall near-infrared non-cadmium quantum dots for in vivo tumor imaging, Small 6 (2) (2010) 256.
[83] S. Santra, H. Yang, P.H. Holloway, J.T. Stanley, R.A. Mericle, Synthesis of water-dispersible fluorescent, radio-opaque, and paramagnetic CdS: Mn/ZnS quantum dots: a multifunctional probe for bioimaging, J. Am. Chem. Soc. 127 (6) (2005) 1656.
[84] E. Pöselt, C. Schmidtke, S. Fischer, K. Peldschus, J. Salamon, H. Kloust, H. Tran, A. Pietsch, M. Heine, G. Adam, Tailor-made quantum dot and iron oxide based contrast agents for in vitro and in vivo tumor imaging, ACS Nano 6 (4) (2012) 3346.
[85] F. Tokumasu, R.M. Fairhurst, G.R. Ostera, N.J. Brittain, J. Hwang, T.E. Wellems, J.A. Dvorak, Band 3 modifications in *Plasmodium falciparum*-infected AA and CC erythrocytes assayed by autocorrelation analysis using quantum dots, J. Cell Sci. 118 (5) (2005) 1091.
[86] F. Patolsky, G. Zheng, O. Hayden, M. Lakadamyali, X. Zhuang, C.M. Lieber, Electrical detection of single viruses, Proc. Natl. Acad. Sci. U. S. A. 101 (39) (2004) 14017.
[87] P.L. Chiang, T.C. Chou, T.H. Wu, C.C. Li, C.D. Liao, J.Y. Lin, M.H. Tsai, C.C. Tsai, C.J. Sun, C.H. Wang, Nanowire transistor-based ultrasensitive virus detection with reversible surface functionalization, Chem. Asian. J. 7 (9) (2012) 2073.

[88] W.U. Wang, C. Chen, K.-H. Lin, Y. Fang, C.M. Lieber, Label-free detection of small-molecule-protein interactions by using nanowire nanosensors, Proc. Natl. Acad. Sci. U. S. A. 102 (9) (2005) 3208.
[89] G. Lee, J. Lim, J. Park, S. Choi, S. Hong, H. Park, Neurotransmitter detection by enzyme-immobilized CNT-FET, Curr. Appl. Phys. 9 (1) (2009) S25.
[90] J.-I. Hahm, C.M. Lieber, Direct ultrasensitive electrical detection of DNA and DNA sequence variations using nanowire nanosensors, Nano Lett. 4 (1) (2004) 51.
[91] G.-J. Zhang, J.H. Chua, R.-E. Chee, A. Agarwal, S.M. Wong, Label-free direct detection of MiRNAs with silicon nanowire biosensors, Biosens. Bioelectron. 24 (8) (2009) 2504.
[92] G.-J. Zhang, L. Zhang, M.J. Huang, Z.H.H. Luo, G.K.I. Tay, E.-J.A. Lim, T.G. Kang, Y. Chen, Silicon nanowire biosensor for highly sensitive and rapid detection of Dengue virus, Sensors Actuators B Chem. 146 (1) (2010) 138.
[93] H.J. Yoon, T.H. Kim, Z. Zhang, E. Azizi, T.M. Pham, C. Paoletti, J. Lin, N. Ramnath, M.S. Wicha, D.F. Hayes, Sensitive capture of circulating tumour cells by functionalized graphene oxide nanosheets, Nat. Nanotechnol. 8 (10) (2013) 735.
[94] C.-W. Lin, K.-C. Wei, S.-S. Liao, C.Y. Huang, C.-L. Sun, P.-J. Wu, Y.-J. Lu, H.-W. Yang, C.-C.M. Ma, A reusable magnetic graphene oxide-modified biosensor for vascular endothelial growth factor detection in cancer diagnosis, Biosens. Bioelectron. 67 (2015) 431.
[95] D. Du, L. Wang, Y. Shao, J. Wang, M.H. Engelhard, Y. Lin, Functionalized graphene oxide as a nanocarrier in a multienzyme labeling amplification strategy for ultrasensitive electrochemical immunoassay of phosphorylated p53 (S392), Anal. Chem. 83 (3) (2011) 746.
[96] S. Kumar, S. Kumar, S. Srivastava, B.K. Yadav, S.H. Lee, J.G. Sharma, D.C. Doval, B.D. Malhotra, Reduced graphene oxide modified smart conducting paper for cancer biosensor, Biosens. Bioelectron. 73 (2015) 114.
[97] A.L. West, M.H. Griep, D.P. Cole, S.P. Karna, DNase 1 retains endodeoxyribonuclease activity following gold nanocluster synthesis, Anal. Chem. 86 (15) (2014) 7377.
[98] L.-L. Wang, J. Qiao, H.-H. Liu, J. Hao, L. Qi, X.-P. Zhou, D. Li, Z.-X. Nie, L.-Q. Mao, Ratiometric fluorescent probe based on gold nanoclusters and alizarin red-boronic acid for monitoring glucose in brain microdialysate, Anal. Chem. 86 (19) (2014) 9758.
[99] K.S. Park, S.S. Oh, H.T. Soh, H.G. Park, Target-controlled formation of silver nanoclusters in abasic site-incorporated duplex DNA for label-free fluorescence detection of theophylline, Nanoscale 6 (17) (2014) 9977.
[100] J. Peng, L.N. Feng, K. Zhang, X.H. Li, L.P. Jiang, J.J. Zhu, Calcium carbonate-gold nanocluster hybrid spheres: synthesis and versatile application in immunoassays, Chem. A Eur. J. 18 (17) (2012) 5261.
[101] L.V. Nair, S.S. Nazeer, R.S. Jayasree, A. Ajayaghosh, Fluorescence imaging assisted photodynamic therapy using photosensitizer-linked gold quantum clusters, ACS Nano 9 (6) (2015) 5825.
[102] S. Gao, D. Chen, Q. Li, J. Ye, H. Jiang, C. Amatore, X. Wang, Near-infrared fluorescence imaging of cancer cells and tumors through specific biosynthesis of silver nanoclusters, Scientific Rep. 4 (2014).
[103] Y. Wang, Y. Cui, R. Liu, Y. Wei, X. Jiang, H. Zhu, L. Gao, Y. Zhao, Z. Chai, X. Gao, Blue two-photon fluorescence metal cluster probe precisely marking cell nuclei of two cell lines, Chem. Commun. 49 (91) (2013) 10724.